Letter of Intent to Jefferson Lab PAC30

Anti-shadowing and the EMC Effect at very large x.

J. Arrington (Spokesperson), D. F. Geesaman, K. Hafidi,
R. J. Holt, D. H. Potterveld, P. E. Reimer, P. Solvignon
Argonne National Laboratory, Argonne, IL

A. Bruell (Spokesperson), R. Ent, H. Fenker, D. Gaskell, M.
Jones, A. F. Lung, D. J. Mack, D. G. Meekins, J. Roche, G. Smith
Jefferson Laboratory, Newport News, VA

M. E. Christy, C. E. Keppel, L. Tang, V. Tvaskis
Hampton University, Hampton, VA

H. Mkrtchyan, T. Navasardyan, V. Tadevosyan
Yerevan Physics Institute, Armenia

(Dated: July 7, 2006)

Abstract

We propose to measure inclusive electron scattering from ^{2}H and several nuclei spanning the mass range from ^{3}He to Au, with an emphasis on the anti-shadowing region ($0.1 < x < 0.3$) and, to a lesser degree, data at extremely large x values. Data in the anti-shadowing region are limited, and do not provide a clear measurement of the A dependence of the effects in this region. Higher precision data in this region, combined with upcoming Drell-Yan measurements of the anti-quark ratios in the same kinematic regime, will allow for better separation of the nuclear dependence of quark, antiquark, and gluon distributions at low x.

In the large x region, the rising EMC ratio as x approaches 1 is attributed to binding and Fermi motion effects. Mean–field calculations in this region describe the qualitative behavior rather well while often failing quantitatively. Additional measurements for $x > 0.85$, as well as in few-body nuclei, will allow much better tests of realistic binding calculations. In addition, the ratios at $x > 1$ are much more sensitive to certain models of for the EMC effect which are difficult to test in other observables. The energy available after the 12 GeV upgrade, combined with the high luminosity available at Jefferson Lab, will allow us to significantly improve the data in the anti-shadowing region and at extremely large x values.

I. INTRODUCTION AND MOTIVATION

We proposed to make new measurements of the nuclear dependence of the structure functions for a range of nuclei. Current data in the anti-shadowing region is rather limited, and new measurements will allow for a much better measurement of the x and A dependence for $x < 0.3$. This will be particularly useful in light of the high precision measurements of the nuclear dependence of the anti-quark distributions that will be provided by the Fermilab E906 Drell-Yan measurement. Several analyses (e.g. Ref. [1–3]) have examined nuclear dependence measurements in DIS along with results from Drell-Yan measurement [4], which are sensitive to the anti-quark distributions, and/or neutrino scattering [5, 6]. In addition, information on the nuclear dependence of the glue can be extracted from measurements of the Q^2 dependence of the nuclear structure functions [7] as well as J/Ψ production from nuclei [8]. Such combined analyses have attempted to isolate nuclear effects in the valence quarks, sea quarks, and gluon distributions in nuclei, with much of the emphasis on the shadowing region. With new measurements planned for the nuclear dependence in the anti-quark distributions (Fermilab E906), and high precision measurements of nuclear effects in neutrino scattering (MINERνA), such combined analysis will have greater ability to isolate the different contributions, in particular in the anti-shadowing region, providing greater interest in high precision measurements of the x and A dependence in DIS scattering.

In addition, modern calculations demonstrate that binding effects are important even at the low x values of the EMC effect and into the anti-shadowing region. This implies that, whatever the cause of the enhancement in the anti-shadowing region, the effect is larger than one would deduce from simply taking the deviation from unity. While existing anti-shadowing measurements do not show the same A dependence observed at larger x (and typically assumed in global fits), this could well be due in part to cancellation between the nuclear dependence of suppression due to binding and enhancement due to, e.g. nuclear pions, in the low x region. It is important to have precision data throughout this low x region, even in the region where no nuclear dependence is observed.

The large x data will provide important tests of binding calculations, by making precise measurements in the region where binding effects are large, and by providing measurements on few-body nuclei, where more reliable calculations of binding can be tested against the the new, high precision, data. Preliminary results from the recently completed E03-103 measurement indicate that one can make precise measurements of the EMC effect at large x by relaxing the typical requirement for DIS kinematics. The existing data extend to $x = 0.65(0.75)$ for $W^2 > 4(3)$ GeV^2, while measurements at 11 GeV will reach $x = 0.8$ in the DIS region, and $x = 0.85$ for $W^2 > 3$ GeV^2. Thus, we can make precise measurements of the EMC effect over the entire region where binding and Fermi motion are believed to be the dominant effects.

Finally, some models of the EMC effect that include medium modification to the nucleon structure predict that for $x \gtrsim 1$, there will be nuclear effects that are much larger than those observed at moderate x values. These measurements have great sensitivity to explanations of the EMC effect in terms of non-hadronic degrees of freedom, and measurements at $x > 1$ may be the best way to provide evidence for such explanations, or set limits that would exclude these effects as being relevant in the region of the EMC effect.

II. TECHNICAL PARTICIPATION OF RESEARCH GROUPS

This lead institutions for this proposal are Argonne National Lab and the Jefferson Lab. The Medium Energy Physics group at Argonne has responsibility for the initial optics design of the SHMS, field maps and verification of the optics of the SHMS.

III. NUCLEAR DEPENDENCE OF THE STRUCTURE FUNCTIONS

A. Overview

Since the original observation of the modification of structure functions in nuclei by the European Muon Collaboration [9], there has been intense theoretical and experimental activity aimed at understanding nuclear effects in parton distribution functions. Twenty years later, these nuclear effects are still not fully understood. Several reviews of the EMC effect have appeared in the literature (for example, see [10–12]), so we will not focus on a detailed description here, but review some of the main features, in particular as they pertain to this proposal.

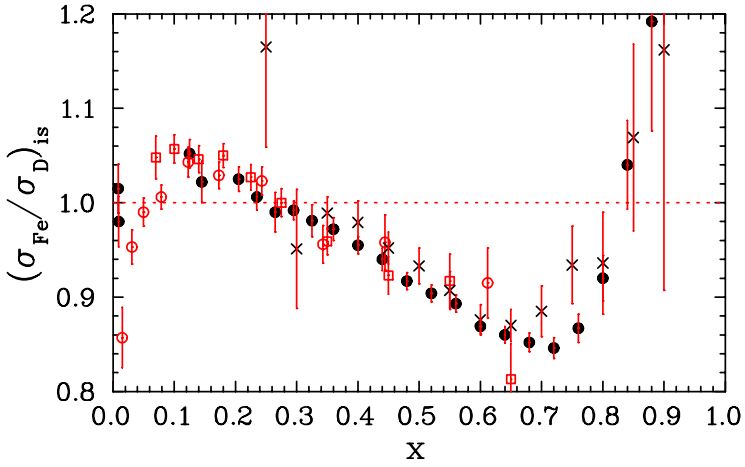

FIG. 1: (σ_A/σ_{2H}) ratios as a function of x from EMC (hollow circles), SLAC (crosses and solid circles), and BCDMS (squares). The data have been averaged over Q^2 and corrected for neutron excess. The SLAC and BCDMS points show $(\sigma_{Fe}/\sigma_{2H})$ while the EMC points show $(\sigma_{Cu}/\sigma_{2H})$

Figure 1 shows the ratio of the inclusive lepton deep inelastic cross section from iron to that from deuterium as measured by the EMC collaboration [9], the BCDMS collaboration [13], and SLAC experiments E87 [14] and E139 [15]. The x-dependence of the cross section ratio is typically broken down into three regions: the region $x < 0.1$, where the nuclear cross section is suppressed (the shadowing region), the small enhancement at $0.1 < x < 0.3$ (the anti-shadowing region), and the large suppression at $x > 0.3$ (the "EMC effect" region). There is, in addition, a fourth region at $x > 0.7$ where the EMC ratio increases and becomes larger than 1.0 at $x \approx 0.8$.

High precision measurements have been made primarily in the shadowing region and in the EMC effect region. In the shadowing region, the nuclear dependence of the structure function is large, and the effects have been mapped out in some detail in high energy measurements. The suppression of the quark distributions at extremely low x can be well

described in terms of shadowing of the partons. In a partonic picture, this can be viewed as the effect overlap of the low x partons which, in accordance with the uncertainty principle, must have a large (longitudinal) spatial distribution. It can also be viewed in terms of fluctuations of the virtual photon into a hadronic system, which can then interact with the nucleus, leading to a masking of the inner nucleons.

In the region of the EMC effect, several experiments have provided detailed information on the A and x dependence of the structure functions, but the interpretation is not as well established as in the shadowing region. The suppression of the quark distributions at large x is at least partially explained by the effects of nuclear binding. However, the uncertainty in calculating the effects of binding makes it difficult to determine if additional effects are needed to explain the data.

B. Large x region

The large x region, $x \gtrsim 0.8$, is often ignored for two reasons. First, there is a lack of high precision data in the large x regime. Second, while most calculations fail to precisely reproduce the data at very large x, it is assumed to be fully described in terms of Fermi motion and binding effects, requiring no new or exotic physics. However, the uncertainty in the calculations and the lack of high quality data in this region make it difficult to test this assumption. It is important to note that these conventional nuclear physics effects are important throughout the full x range of the EMC effect. Precision data at high x can serve as a strict constraint on models that attempt to include standard nuclear effects in other x regions.

Experiment E03-103 [16] has preliminary results for EMC effect measurements on ^{4}He and ^{3}He, covering an x range from 0.3 to 0.85. The larger x data is at $W^2 < 4$ GeV^2, but both the individual structure functions and the ratios are in excellent agreement with previous SLAC measurements in the DIS regime. These data demonstrate quantitatively the ability to reliably extract the nuclear dependence at larger x than previous measurements by relaxing the typical DIS cuts on W^2. Even so, this data is limited to $x = 0.65(0.75)$ for $W^2 > 4(3)$ GeV^2, while measurements at 11 GeV can reach $x = 0.80(0.85)$.

There are indications that one can relax the W^2 condition even further, but there are no precise measurements in the DIS region for these x values, so one must verify that there is no significant Q^2 dependence by measuring the ratio over a range in Q^2. For the E03-103 data, the measured Q^2 dependence is small all the way to $x = 0.85$. Given this, it appears as though the 11 GeV beam will allow us to measure the EMC effect for $x > 1$, which has been shown to be extremely sensitive to some models of the EMC effect [10]. Quark cluster models (e.g. Refs. [17–20]), for example, have been used to explain the excess in the anti-shadowing region. Many approaches have been taken, and while particular approaches require cluster contributions that are unreasonably large, it is difficult to rule out such explanations in general without additional data to test some of the specific predictions of these models. The natural way to test such models is in measurements at $x > 1$. Some cluster models predict large effects in the target ratios for $x \gtrsim 1$, while others predict large effects in the structure function for $x \approx 2$ or $x \approx 3$. The former models can be tested with the large x EMC ratios proposed here, while the latter can be examined with proposed measurements at extremely high x.

C. The Anti-shadowing Region

The anti-shadowing region is also poorly understood, in part because of the limits of the available data, and in part because of the difficulty of making quantitative calculations of the effects of binding to provide a reliable baseline when testing more exotic effects. Some high energy experiments, focussed mainly on the shadowing region, provide measurements in the anti-shadowing region, but these data are typically statistics limited, and do not have the precision necessary to map out the shape or A dependence of the nuclear effects. Data from SLAC, EMC, and BCDMS measurements provide higher precision measurements in this region, but there is scatter among the measurements, and for some experiments, this is the region where large corrections must be applied to the data. Radiative corrections can be a limiting factor for measurements at low x and small scattering angle, while corrections for charge-symmetric backgrounds coming from produced rather than scattered electrons can be extremely large at low x and larger angles. For example, the charge-symmetric background corrections for SLAC E139 [15] reached 10% for deuterium at the lowest x values, and was presumably significantly larger for the high-Z targets. Such corrections can be strongly dependent on the target, and thus have the possibility of introducing an artificial A-dependence to the measurements. Such corrections may explain the scatter in existing measurements, and the fact that there is not a clear A dependence of the ratios in the anti-shadowing regions.

There is little understanding of the explanation for the observed enhancement in the anti-shadowing regime, and even determining the quantitative size of the effect is difficult. At larger x values, nuclear binding is clearly important, and appears to explain much, if not all, of the suppression of the structure function. In the anti-shadowing region, $0.1 < x < 0.3$, binding calculations predict a small suppression of the structure function, meaning that the enhancement observed is not an enhancement of $\sim$ 2–3% relative to the expectation that $\sigma_A/\sigma_D = 1$, but is a larger enhancement. Some early calculations suggested that binding effects were negligible in this region [21, 22], while later calculations predicted effects closer to 5–10% [23–25], with varying predictions for the A dependence of the binding effects for $x < 0.2$ (See Fig. 2). Thus, one needs both high precision data and better calculations of binding effects to understand the size and the A dependence of the enhancement.

There have been several explanations proposed to explain anti-shadowing. It has been described as a consequence of momentum conservation, needed to compensate for the effect of shadowing. However, this does not provide a microscopic explanation of the enhancement. In addition, it has been argued that because one can interpret shadowing as a reaction mechanism effect, the extracted structure function need not satisfy the momentum sum rule. Quark cluster models have also been used to explain anti-shadowing, but the variation of such models makes it difficult to find testicle predictions that can be used to test or rule out this class of models. As mentioned in the previous section, these models are best tested with large x data.

The anti-shadowing region has also been described in terms of the contribution from nuclear pions (mesons), which yield an enhancement over pure binding calculations below $x \approx 0.5$, with larger contributions at very small x values (e.g. Refs. [24–26]). However, such calculations have had difficulty explaining the enhancement in the anti-shadowing region while at the same time explaining the data at larger x and being consistent with the lack of enhancement in the sea quark distributions as measured in Drell-Yan scattering [4].

Rescaling models have also been proposed to explain the enhancement at low x. A

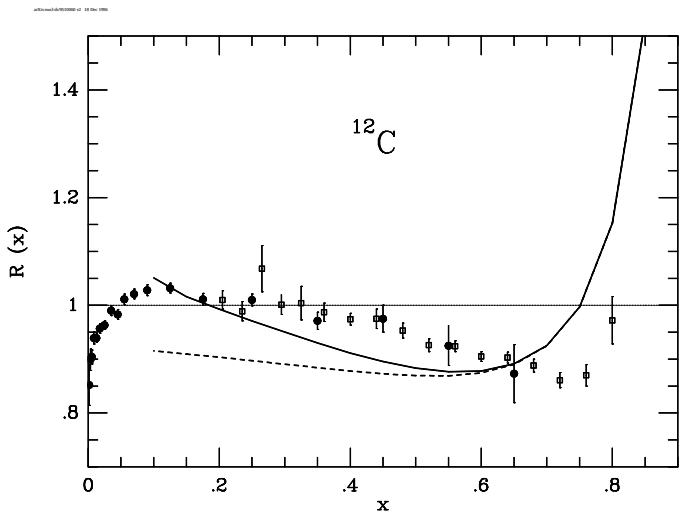

FIG. 2: Calculation of binding (dashed) and binding + nuclear meson contributions (solid) from Marco, et al. [24] for Carbon. Note that $R(x)$ is the ratio of nuclear to *nucleon* structure functions, i.e., ignoring Fermi motion effects in deuterium, which is the reason for the significant disagreement at the large x values.

modification of the Q^2 scale in heavy nuclei relative to deuterium can also provide an effect in the anti-shadowing region, and has been connected to pictures of nucleon "swelling" due to the change in the confinement scale for the bound nucleon. However, there is mainly based on the observation that such a change in the scale could reproduce the effect; there is no external information that indicates how the scale should change. When interpreted in terms of nucleon swelling, the necessary effects appears to be too large to be consistent with other limits on modification to bound nucleons, although the detailed comparison depends on assumptions made in the comparison, e.g. the relationship between the modification of the size and mass of the nucleon.

Little progress has been made in explaining anti-shadowing in the last decade, due to the lack of precise data, and the difficulty in extracting the size of the effect that must be described by these more exotic explanations. However, there has been some work aimed at improving the calculations of binding, examining the EMC effect in new frameworks, and connecting models of the EMC effect to other observables. Liuti and Taneja [27], have examined the EMC effect in the framework of Generalized Patron Distributions (GPDs). In their calculation, anti-shadowing is attributed to off-shell effects, and the GPD framework allows for a connection between the EMC effect and in-medium modification of nucleon form factors [28]. This connection has also been explored by Thomas and collaborators in the Quark-Meson Coupling (QMC) model [29] which was used to study medium modification of in-medium nucleon form factors [30], and then applied to study the EMC effect for both unpolarized [31] and polarized [32, 33] structure functions, as well as other observables for nuclei and nuclear matter [34]. The comparison of polarized and unpolarized EMC effect in nuclear matter [32] shows that the greatest difference between the two cases is in the anti-shadowing region, making this region of particular interest. In addition, calculations for finite nuclei [33] show a significant A dependence in the difference between the polarized and unpolarized EMC effect, further enhancing the need for a precise, systematic study of

the A dependence of anti-shadowing. Recent work by Miller and Smith use a Chiral soliton model to relate nucleon form factor modification [35], the EMC effect in polarized [36] and unpolarized [37, 38] structure functions, and the nuclear dependence of Drell-Yan scattering [38]. In this case, the prediction for the polarized EMC effect again shows the largest difference in the region of anti-shadowing, but the prediction is quite different from the QMC model prediction [32].

There have also been recent examinations of the effects in the shadowing and anti-shadowing region [39] in terms of constructive and destructive interference amplitudes related to quark multiple scattering. This predicts a non-universality to the EMC effect, predicting a different effect for neutral and charged current reactions, which could have an impact on the NuTeV $\sin^2\theta_W$ anomaly [40]. This recent theoretical work, combined with plans to make significantly improved measurements of anti-shadowing in sea quarks using Drell-Yan scattering and high statistics measurements of nuclear effects in neutrino scattering, make improved measurements of anti-shadowing in electron scattering essential.

With new results soon to be available from the JLab measurements of the EMC effect for few-body nuclei, it will be possible to make more accurate comparisons to detailed binding calculations using realistic nuclear structure. This will help to improve models of binding effects and thus establish the "baseline" expectation for the ratio at low x in the absence of effects beyond traditional binding. This, combined with systematic study of the x and A dependence in the low x region will help to quantify the size and x range of the *additional* nuclear effects, allowing us to better evaluate the proposed explanations for the EMC effect. High precision data for ^{3}He and ^{4}He in the anti-shadowing region will be particularly useful. More reliable calculations can be peformed for these few-body nuclei, both for the effects of binding and in the evaluation of additional effects needed to explain anti-shadowing. In addition, the initial results from E03-103 indicate that the EMC effect in ^{4}He is nearly identical to the effect in C, and that the EMC effect in ^{3}He, while smaller, is much larger than predicted by most calculations or models of the A dependence. While the ^{3}He result is very sensitive to the model used to evaluate the ratio of proton to neutron cross section at large x, these results suggest that the nuclear effects are significant, even in these few-body nuclei. It will be very interesting to see if this indication of unusually large effects, even for ^{3}He and ^{4}He holds in the anti-shadowing region as well. Some preliminary results from E03-103 will be presented in the following section.

D. Existing Data

There have been several measurements made of the structure function ratios in the anti-shadowing regime, but the overall quality and coverage of the data is limited compared to the large x or shadowing regions. Measurements by the EMC [9], NMC [41, 42], BCDMS [13, 43] collaborations and experiments at SLAC [14, 15] have all provided information in this region. However, in many cases, the data in the anti-shadowing region were the last points on the low (high) x side of the coverage, and were in some cases limited by statistics or by large systematic effects. Some of the experiments had data on a limited number of targets or had insufficient statistics to make a conclusion about the A dependence. This, combined with the fact that there appears to be some inconsistency between data sets, makes it more difficult to make a global determination of the A dependence. Finally, while global fits often assume an identical A dependence for the anti-shadowing and EMC regions, this dependence is not clear in the data. The NMC measurement [42] shows essentially no effect in ^{6}Li, but

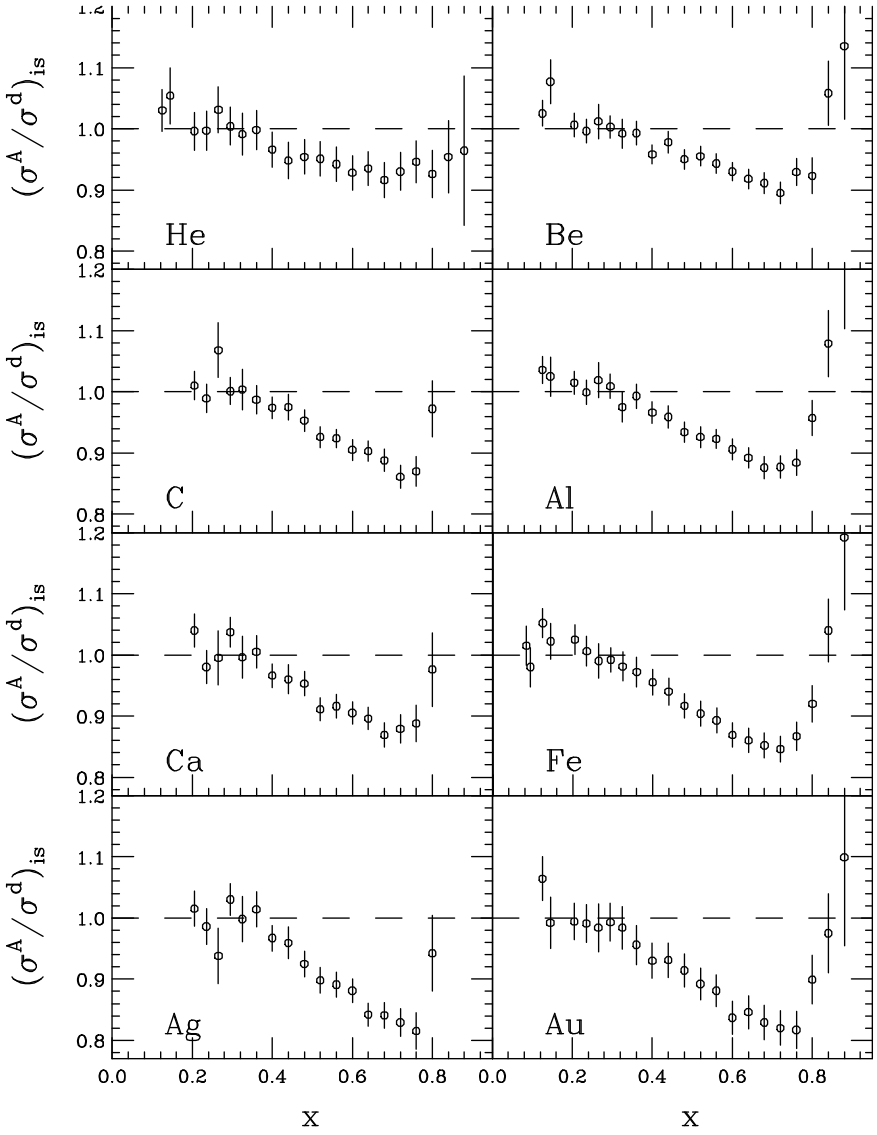

FIG. 3: (σ_A/σ_{2H}) ratios as a function of x from SLAC E139 for several nuclei. The data have been averaged over Q^2 and corrected for neutron excess.

a clear effect of 2–3% in C, while the E139 data (Fig. 3) appear to show anti-shadowing in Fe, but not for heavier nuclei. Because of the limited and and sometimes contradictory evidence, a high precision, systematic study of the anti-shadowing region is necessary. We will provide high precision measurements for a wide range of nuclei in this region, including ^{3}He and ^{4}He.

Global analyses have combined these DIS measurements with Drell-Yan data and neutrino-nucleus scattering to try and separate nuclear effects on valence quarks, sea quarks, and the gluons. New measurements for the nuclear dependence in Drell-Yan scattering will be made by FNAL E906 (Fig. 4) , with a significant improvement in the precision over the entire anti-shadowing region. Previous measurements by E772 [4] have a poor precision over this x range, and while they show some indication of shadowing for $x \approx 0.05$, the uncertainties are much larger than those for DIS measurements in the anti-shadowing region.

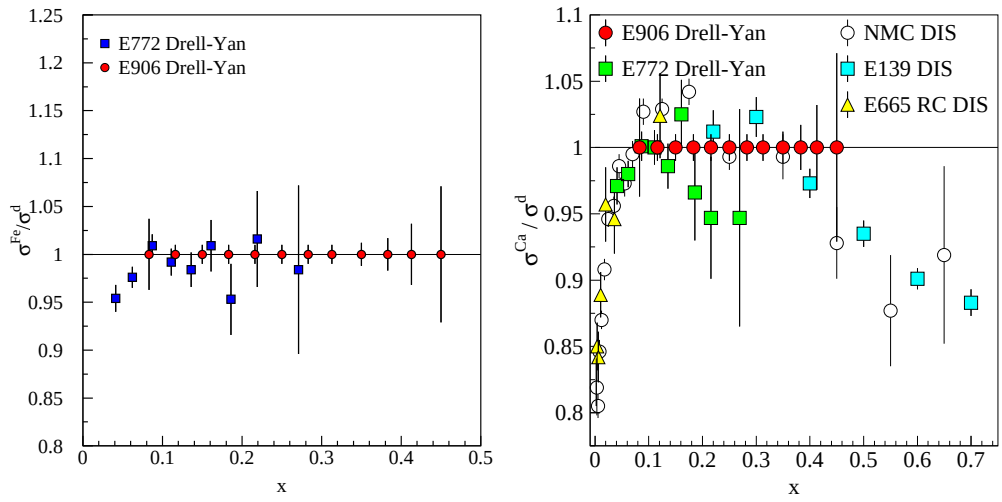

FIG. 4: Left: Drell-Yan measurements of the EMC effect for anti-quarks from previous E772 measurements, along with the projected uncertainties for the proposed E906 measurements. Right: Previous and proposed Drell-Yan measurements of the anti-quark ratios, compared to DIS measurements.

These data were able to rule out some nuclear pion models which predicted a much larger effect in the anti-quark distributions than in the DIS measurements. However, several more recent calculations show smaller contributions to the Drell-Yan measurement from nuclear pions, and the data are not precise enough to be sensitive to anti-shadowing of the same magnitude as is observed in DIS, as seen in the rightmost plot in Fig. 4. In addition, the MINERνA experiment at Fermilab plans to make measurements of the nuclear dependence in ν-A scattering, which provides additional sensitivity to the flavor dependence of the quark distributions.

The most complete measurements of the EMC effect in the large x region come from SLAC experiment E139 [15]. They measured ratios to deuterium for ^{4}He, ^{9}Be, C, Al, Ca, Fe, Ag, and Au targets. They found no significant Q^2-dependence in the measured cross section ratios and, as seen in Fig. 3, there is an A dependence to the *size* of the suppression, but no apparent change in the *shape* of the cross section ratios as a function of x. The A dependence in the size of the effect can be described equally well as a simple function of A, or as a function of the average nuclear density.

Experiment E03-103 [16] took advantage of the observed scaling of the nuclear structure functions [44–46], even for $W^2 < 4$ GeV^2, to make higher precision measurements of the EMC effect at large x. The emphasis was on few-body nuclei, where binding calculations can be tested with reduced uncertainty coming from the uncertainty in the nuclear structure, and large x, where these binding effects are expected to dominate. Figure 5 shows the preliminary measurement of the EMC effect in carbon, for five different Q^2 values between 3 and 5 GeV^2 at $x = 0.6$. The data sets at different Q^2 values do not show any systematic Q^2 dependence, and the scatter at the largest x values is both consistent with the uncertainties in the individual measurements and much smaller than the statistical uncertainties from previous measurements.

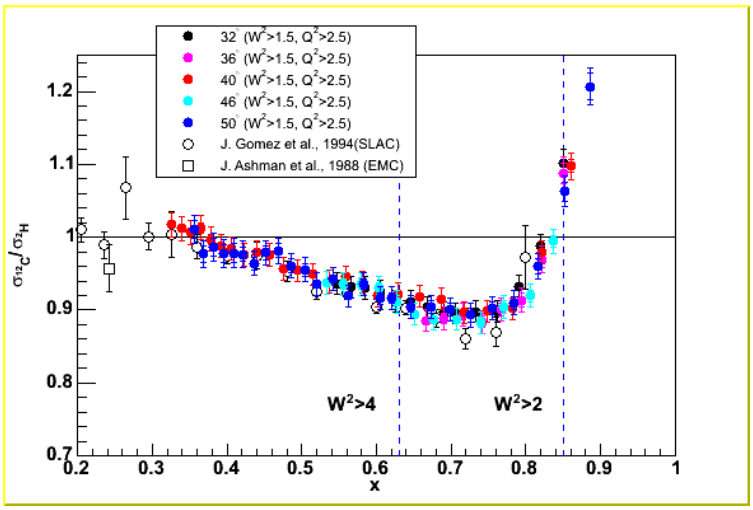

FIG. 5: (σ_C/σ_{2H}) ratios as a function of x from E03-103 (colored circles) for five different Q^2 values. The dashed lines indicate the cutoff for W^2 values of 4 and 2 GeV^2. The results are consistent with the SLAC E139 measurements, taken entirely in the DIS region, and have much high precision in the large x region.

IV. PROPOSED KINEMATIC COVERAGE

This experiment will measure the EMC effect for nuclei from ^{3}He to Au, for $0.1 < x \lesssim 1$, with $Q^2 > 2$ GeV^2 in the anti-shadowing region (large W^2) and $Q^2 \gtrsim 10$ GeV^2 for $x > 0.5$. In addition, the structure functions and EMC ratios at large x will be measured as a function of Q^2 for a subset of the targets to verify that there is no Q^2 dependence in the measured ratio for the largest x values.

Figure 6 shows the proposed kinematic coverage at 11 GeV ($\theta \leq 45^\circ$) as a function of x and Q^2. The solid blue points denote the x–Q^2 region for which we will take data for all nuclear targets and extract the EMC effect. The solid and dashed blue lines mark the $W^2 = 4$ GeV^2 and $W^2 = 2$ GeV^2 limits. For many of the SLAC kinematics shown, in particular the largest x values, the statisical uncertainty of the extracted EMC ratios is very large. For E03-103, we exclude measurements beyond $x = 0.85$ because the statistical uncertainties in the ratios start to become significantly larger, and because the verification of the Q^2 independence of the result much less precise.

V. EXPERIMENTAL REQUIREMENTS

We propose a measurement of inclusive electron scattering from deuterium, ^{3}He, ^{4}He and several heavy nuclei spanning ^{7}Li to Au. Scattered electrons will be measured in the HMS and SHMS spectrometers, which will run independently. The majority of the anti-shadowing data will be taken with the SHMS, while the HMS and SHMS will both take data at the larger angles, covering the large x, high Q^2 part of the measurement. Measurements in the anti-shadowing region will be taken at 20, 25, and 30 degrees scattering angles. At 30 degrees, the charge symmetric background will be the greatest, almost 50% of the scattered electron rate for the thickest targets at the lowest x value. The background us much smaller

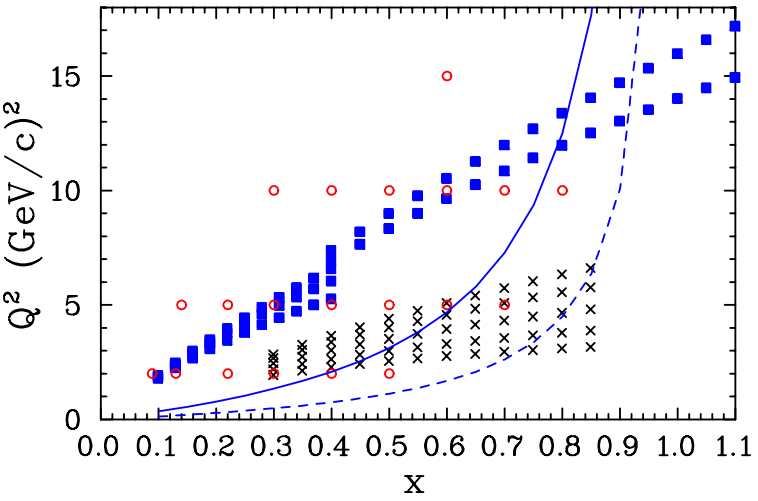

FIG. 6: Overview of the proposed kinematics. The solid blue squares are the kinematics of the proposed measurement for all targets. The black 'x's are the the kinematics from E03-103, and the hollow red circles indicate the SLAC E139 kinematics. In addition to the points shown, we will take additional measurements at large x for Q^2 between 6 and 12 GeV^2 to quantify the x region over which the EMC ratios are independent of Q^2.

for the lighter targets, and drops rapidly as one increases x or decreases the scattering angle. Similarly, radiative corrections (primarily the contribution of low-Q^2 quasielastic events radiating into the low x tails) become large for the lowest x values at small scattering angles. Based on the extensive measurements at low x and Q^2 at 6 GeV from the E99-118 measurement, we are confident that we can apply these corrections reliably for the angles where measurements are proposed. By taking measurements at multiple scattering angles, we can test the radiative corrections, charge-symmetric backgrounds, and rate-dependent effects. We believe that we can adequately treat all of these corrections at all three angles, but having all three measurements will allow us to test this. As the rates are large for the lower scattering angles, the additional angles take little additional time.

We will make extensive measurements of electrons from background (charge symmetric) processes We will take data at 35 and 45 degrees, over a range of scattered electron energies covering $0.4 < x < 1.1$ in 20 bins. Data will be taken on deuterium, helium-3, helium-4, lithium, beryllium, carbon, aluminum, calcium, copper, silver, and gold, as well as a separate, dummy aluminum target (for subtraction of the target endcap contributions). Data will be taken at four additional angles for a subset of targets (deuterium, C, and Cu) to check the Q^2-dependence of the extracted EMC ratio. We will also take hydrogen elastic data for calibration, as well as performing several BCM calibrations and studies of target boiling effects for the hydrogen and helium targets. This measurement uses the standard target systems and the base HMS and SHMS detector packages.

Table I lists the kinematics we propose to measure, corresponding to the kinematics shown in Fig. 6. Target and momentum changes are included in the total time at each scattering angle. In all cases, data will be obtained utilizing 4 cm deuterium, an aluminum 'dummy' target and several solid targets. Most of the solid targets that will be used have been used in previous Hall C experiments. One notable exception is the ^{7}Li target. For this target only, we will require that the target be in thermal contact with the cryotarget ladder, rather

θ (deg)	E' (GeV)	x	Q^2 (GeV^2)	time (hours)
40	1.3-3.0 (3 settings)	0.4-1.1	6-14	~100 - SHMS
50	1.0-2.2 (5 settings)	0.4-1.1	7-16	(~200) - HMS
20	2.0-4.5 (4 settings)	0.1-0.4	2-5	~60 - SHMS
25	1.7-3.5 (4 settings)	0.1-0.4	3-6	~60 - SHMS
30	1.5-2.7 (3 settings)	0.1-0.4	3-7	~60 - SHMS
				~280*1.3*1.1=400 hrs

TABLE I: Kinematics for the proposed measurements. All data will be taken at 11 GeV beam energy. The run time for the large x measurements includes time for all targets at 40 and 50 degrees, and three targets at 20, 25, 30, and 35 degrees. Additional dummy running and charge-symmetric background measurements will increase the total runtime by ~30%, and overhead for configuration changes will be about 10% more.

than be placed on a separate solid target ladder as is commonly done in Hall C. This will allow us to run higher currents without undo heating of the lithium target material. Even so, we estimate that we will be able to run at most 25 μA on a rather thin (100 mg/cm^2) target.

We will run at currents between 25 and 80 μA with 11 GeV beam energy. Table II is a summary of the estimated beam time required for the measurement. The bulk of the runtime is for SHMS measurements in the anti-shadowing region, with some time allocated to cover the larger x range and make measurement that overlap the previous measurements. The HMS is mainly running parasitically, taking data at the large x and Q^2 values, along with some quick measurements of the Q^2 dependence at large x for two targets. Run times have been estimated assuming at least 1% statistics in each x bin for each target (double statistics for deuterium, which generally has a shorter run time). In addition to the data acquisition time, we have allocated time for checkout and background measurements, and spectrometer angle changes.

We estimate a systematic uncertainty of $\approx$3% in the measured cross sections for most of the kinematics. To correct for density changes due to localized heating in the deuterium target, we will measure rate as a function of current. Many sources of uncertainty will cancel in the cross section ratios for different targets, and we estimate a final point–to–point systematic uncertainty in the ratios of approximately 0.6% and an overall scale systematic uncertainty of 1–2%. Table III shows the contributions to the systematic uncertainties in the target ratios. Note that the uncertainty in the thickness of the deuterium target is a common uncertainty for the $\sigma_A/\sigma_{^2H}$ ratios for all targets.

Activity	Time (hours)
Production Running	~400
Q^2 dependence for ^{2}H,C,Cu	24
Target Boiling Studies	16
BCM calibrations	8
Beam spot monitoring	4
Hydrogen elastics	16
checkout/calibration	24
Total	492 (21 days)

TABLE II: Approximate beam time required for the proposed experiment. The time shown is for SHMS running, HMS running will be done simultaneously.

Source	Absolute Uncertainty	Relative Uncertainty	$\delta\sigma/\sigma(\%)$	$\delta R/R(\%)$ point-to-point	$\delta R/R(\%)$ scale	$\delta R/R$ (%) Statistical
HMS Momentum	<0.1%	0.01%	0.2	-	-	
Beam Energy	<0.1%	<0.02%	0.2	-	-	
θ	0.5mr	0.2mr	0.1	-	-	
Beam angle	0.5mr	0.1mr	0.1	-	-	
t_D	0.5%		0.5	-	0.5	
t_A	0.5–2.0%		0.5–2.0	-	0.5–2.0	
Charge	0.4%	0.2%	0.5	0.2	0.2	
Target Boiling	<0.5%	0.2%	<0.5	0.1	0.2	
Endcap Subtraction	<1.0%	0.2%	<1.0	0.1	0.1	
Acceptance	1.0-2.0%	0.2%	1.0-2.0	0.2	0.2	
Radiative Corrections	2.0%	0.5%	2.0	0.2–0.4	0.4	
Detector Efficiency	0.5%	0.2%	0.5	0.2	-	
Deadtime Correction	<0.5%	0.2%	<0.5	0.1	0.2	
Positron Background	0.2%	0.2%	0.2	0.1–0.3	0.2	
Total			2.5-3.2	0.5–0.6	0.9–2.2	0.3-1.2
E139			2.4-3.7	0.3-1.3	1.0-2.5	0.5-11.0

TABLE III: Systematic uncertainties in the ratio $\sigma_A/\sigma_{^2H}$, compared to E139 uncertainties. For $x < 0.9$, the statistical uncertainties will be 0.3–1.2%. The point–to–point systematic error in the target ratios will be 0.5–0.6% and the overall systematic error will range from 0.9–2.2%, depending on the target.

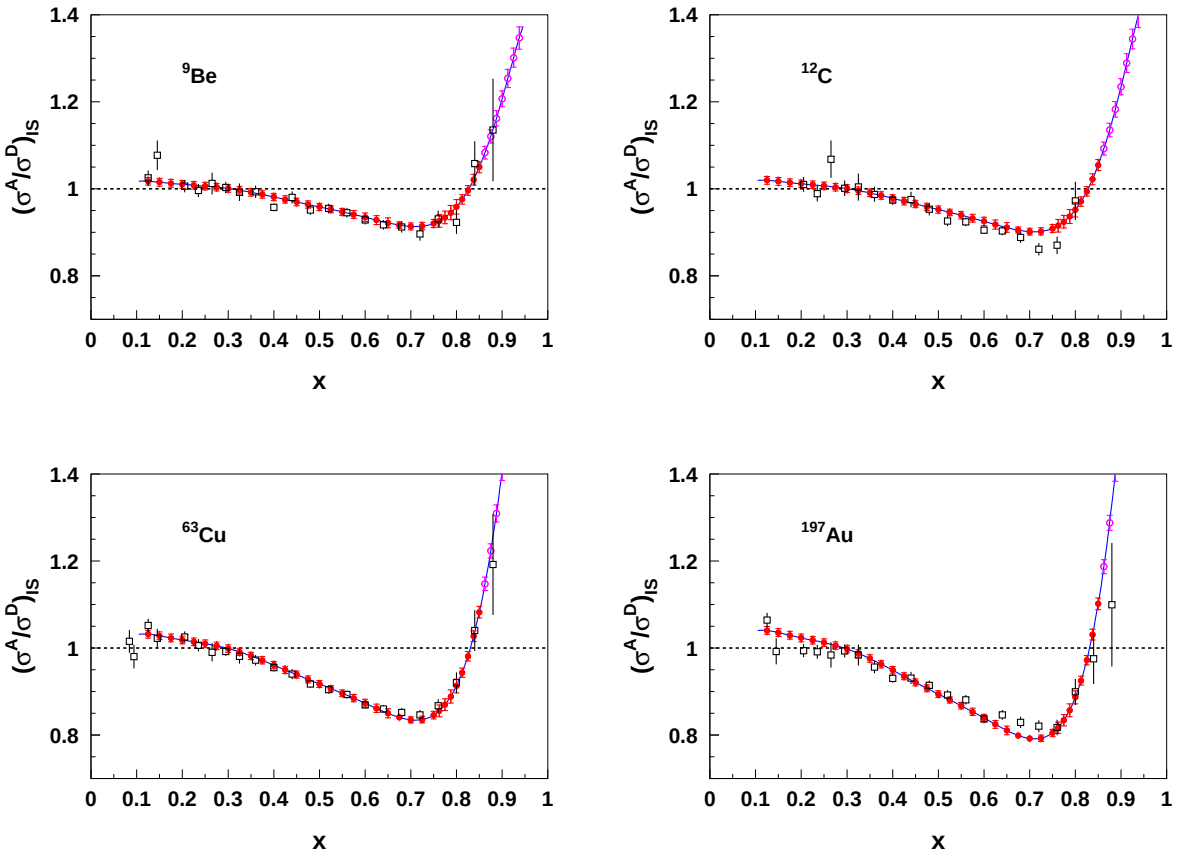

FIG. 7: Projected uncertainties for the ^{9}Be, C, Cu, and Au EMC ratios (colored circles). The inner error bars are statistical, while the outer errors are combined statistics and point–to–point errors. Not shown is an overall $\approx 1-2\%$ systematic uncertainty. The solid red circles are point taken with $W^2 > 4$ GeV^2, while the hollow magenta points are $W^2 > 3$ GeV^2. Also shown are the data from SLAC E139 (open squares), along with their parameterization of the x-dependence (solid line). Note that some of our projected data points are off the scale at high x.

VI. SUMMARY

We will require approximately 21 days in Hall C to measure inclusive scattering from deuterium, ^{3}He, ^{4}He, ^{7}Li, ^{9}Be, C, Al, Ca, Cu, Ag, Au for $0.1 < x \lesssim 1$. We will take additional data on a deuterium, C, and Cu to examine the Q^2-dependence of the nuclear structure functions and the EMC ratio. This measurement takes advantage of the observed equivalence of the EMC effect as measured in the canonical DIS regime and as measured in the resonance region. We will measure the EMC effect with high precision at large x, and we will precise measurements of the x and A dependence in the anti-shadowing region, providing comparable coverage and precision to the anti-quark ratios that will be measured in Drell-Yan scattering in Fermilab E906 in the same x range.

Acknowledgments

This work was supported by the U. S. Department of Energy, Nuclear Physics Division, under contracts W-31-109-ENG-38 and DE-AC05-84ER40150.

---

[1] K. J. Eskola, V. J. Kolhinen, and P. V. Ruuskanen, Nucl. Phys. **B535**, 351 (1998).
[2] M. Hirai, S. Kumano, and T. H. Nagai, Phys. Rev. **C70**, 044905 (2004).
[3] S. A. Kulagin and R. Petti, Nucl. Phys. **A765**, 126 (2006).
[4] D. M. Alde et al., Phys. Rev. Lett. **64**, 2479 (1990).
[5] V. A. Radescu (NuTeV) (2004), hep-ex/0408006.
[6] R. Petti (NOMAD) (2004), hep-ex/0411032.
[7] T. Gousset and H. J. Pirner, Phys. Lett. **B375**, 349 (1996).
[8] P. Amaudruz et al. (New Muon), Nucl. Phys. **B371**, 553 (1992).
[9] J. Aubert et al., Phys. Lett. B **123**, 275 (1983).
[10] M. Arneodo, Phys. Rept. **240**, 301 (1994).
[11] D. F. Geesaman, K. Saito, and A. W. Thomas, Ann. Rev. Nucl. Sci. **45**, 337 (1995).
[12] P. R. Norton, Rept. Prog. Phys. **66**, 1253 (2003).
[13] A. C. Benvenuti et al. (BCDMS), Phys. Lett. B **189**, 483 (1987).
[14] A. Bodek et al., Phys. Rev. Lett. **50**, 1431 (1983).
[15] J. Gomez et al., Phys. Rev. D **49**, 4348 (1994).
[16] J. Arrington, D. Gaskell, et al., Jefferson lab experiment E03-103.
[17] C. E. Carlson and T. J. Havens, Phys. Rev. Lett. **51**, 261 (1983).
[18] B. C. Clark, S. Hama, B. Mulligan, and K. Tanaka, Phys. Rev. **D31**, 617 (1985).
[19] H. Faissner, B. R. Kim, and H. Reithler, Phys. Rev. Lett. **54**, 1902 (1985).
[20] K. E. Lassila and U. P. Sukhatme, Phys. Lett. **B209**, 343 (1988).
[21] S. V. Akulinichev, S. A. Kulagin, and G. M. Vagradov, Phys. Lett. **B158**, 485 (1985).
[22] G. L. Li, K. F. Liu, and G. E. Brown, Phys. Lett. **B213**, 531 (1988).
[23] F. Gross and S. Liuti, Phys. Rev. C **45**, 1374 (1992).
[24] E. Marco, E. Oset, and P. Fernandez de Cordoba, Nucl. Phys. **A611**, 484 (1996).
[25] O. Benhar, V. R. Pandharipande, and I. Sick, Phys. Lett. **B410**, 79 (1997).
[26] D. de Florian, L. N. Epele, H. Fanchiotti, C. A. Garcia Canal, and R. Sassot, Z. Phys. **A350**, 55 (1994).
[27] S. Liuti and S. K. Taneja, Phys. Rev. **C72**, 034902 (2005).
[28] S. Liuti (2006), hep-ph/0601125.
[29] K. Saito and A. W. Thomas, Phys. Lett. **B327**, 9 (1994).
[30] D.-H. Lu, A. W. Thomas, and A. G. Williams, Phys. Rev. **C57**, 2628 (1998).
[31] H. Mineo, W. Bentz, N. Ishii, A. W. Thomas, and K. Yazaki, Nucl. Phys. **A735**, 482 (2004).
[32] I. C. Cloet, W. Bentz, and A. W. Thomas, Phys. Rev. Lett. **95**, 052302 (2005).
[33] I. C. Cloet, W. Bentz, and A. W. Thomas (2006), nucl-th/0605061.
[34] K. Saito, K. Tsushima, and A. W. Thomas (2005), hep-ph/0506314.
[35] J. R. Smith and G. A. Miller, Phys. Rev. **C70**, 065205 (2004).
[36] J. R. Smith and G. A. Miller, Phys. Rev. **C72**, 022203 (2005).
[37] J. R. Smith and G. A. Miller, Phys. Rev. C **65**, 055206 (2002).
[38] J. R. Smith and G. A. Miller, Phys. Rev. Lett. **91**, 212301 (2003).

[39] S. J. Brodsky, I. Schmidt, and J.-J. Yang, Phys. Rev. **D70**, 116003 (2004).
[40] G. P. Zeller et al. (NuTeV), Phys. Rev. Lett. **88**, 091802 (2002).
[41] P. Amaudruz et al. (New Muon), Nucl. Phys. **B441**, 3 (1995).
[42] M. Arneodo et al. (New Muon.), Nucl. Phys. **B441**, 12 (1995).
[43] G. Bari et al. (BCDMS), Phys. Lett. **B163**, 282 (1985).
[44] B. W. Filippone et al., Phys. Rev. C **45**, 1582 (1992).
[45] J. Arrington et al., Phys. Rev. C **64**, 014602 (2001).
[46] J. Arrington, R. Ent, C. E. Keppel, J. Mammei, and I. Niculescu, Phys. Rev. **C73**, 035205 (2006).